THE JOURNAL OF PHYSICAL CHEMISTRY B

pubs.acs.org/JPCB Article

Distinguishing Mesoscale Polar Order (Unidirectional vs Bidirectional) of Cellulose Microfibrils in Plant Cell Walls Using Sum Frequency Generation Spectroscopy

Mohamadamin Makarem, Yoshiharu Nishiyama, Xiaoran Xin, Daniel M. Durachko, Ying Gu, Daniel J. Cosgrove, and Seong H. Kim*

Cite This: J. Phys. Chem. B 2020, 124, 8071−8081 Read Online

ABSTRACT: Cellulose in plant cell walls are synthesized as crystalline microfibrils with diameters of 3−4 nm and lengths of around 1−10 μm. These microfibrils are known to be the backbone of cell walls, and their multiscale three-dimensional organization plays a critical role in cell wall functions including plant growth and recalcitrance to degradation. The mesoscale organization of microfibrils over a 1−100 nm range in cell walls is challenging to resolve because most characterization techniques investigating this length scale suffer from low spatial resolution, sample preparation artifacts, or inaccessibility of specific cell types. Here, we report a sum frequency generation (SFG) study determining the mesoscale polarity of cellulose microfibrils in intact plant cell walls. SFG is a nonlinear optical spectroscopy technique sensitive to the molecular-to-mesoscale order of noncentrosymmetric domains in amorphous matrices. However, the quantitative theoretical model to unravel the effect of polarity in packing of noncentrosymmetric domains on SFG spectral features has remained unresolved. In this work, we show how the phase synchronization principle of the SFG process is used to predict the relative intensities of vibrational modes with different polar angles from the noncentrosymmetric domain axis. Applying this model calculation for the first time and employing SFG microscopy, we found that cellulose microfibrils in certain xylem cell walls are deposited unidirectionally (or biased in one direction) instead of the bidirectional polarity which was believed to be dominant in plant cell walls from volume-averaged characterizations of macroscopic samples. With this advancement in SFG analysis, one can now determine the relative polarity of noncentrosymmetric domains such as crystalline biopolymers interspersed in amorphous polymer matrices, which will open opportunities to study new questions that have not been conceived in the past.

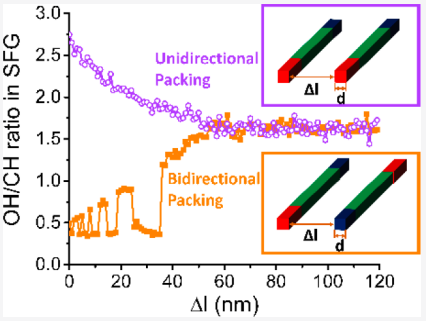

INTRODUCTION

In plants, cell walls consist of cellulose microfibrils (CMFs) and various types of polysaccharides. The elementary CMFs are synthesized and deposited by the cellulose synthase complexes (CSCs) moving in the plasma membrane of the cell.[1,2] In each elementary CMF, the directionality of β-1→4 glycosidic bonds from the reducing end to the nonreducing end is the same for all chains.[1] Thus, the spatial arrangement as well as the overall directionality of CMFs in plant cell walls can provide information about the spatial distribution and movement of CSCs in the cell membrane during the CMF synthesis, which is directly coupled with the biological and mechanical function of the cells in various tissues in plants.[3−6] The cellulose structures also play a critical role in the recalcitrance of lignocellulosic biomass in enzymatic and chemical conversion to other useful forms of chemicals.[7−9]

Plant cell walls are divided into two types: a primary cell wall (PCW) which can expand during the growth of the cell and a secondary cell wall (SCW) which undergoes wall thickening after cell growth and expansion have ceased.[10] In the PCW, CSCs are mostly isolated and move individually along the microtubules beneath the plasma membrane.[11] On the basis of the literature reported so far, the CSCs in PCWs move bidirectionally with almost equal probabilities of the opposite directions of the microtubule.[12] PCWs have a crossed-polylamellate structure; in each lamella, CMFs are deposited along a dominant direction with some local variances and the dominant direction varies from lamella to lamella.[13] Several experimental evidences suggest that CSCs in SCWs move collectively in clusters or certain geometric arrays.[10,14−16] SCWs are usually composed of S1, S2, and S3 layers.[15] Among these, the S2 layers are normally the thickest and the CMFs in the S2 layer are highly aligned at a specific angle, called the microfibril angle (MFA), with respect to the longitudinal axis

Received: August 3, 2020
Revised: August 16, 2020
Published: August 17, 2020

https://dx.doi.org/10.1021/acs.jpcb.0c07076
J. Phys. Chem. B 2020, 124, 8071−8081

of the cell.[17] If the CSCs in SCWs also move bidirectionally along the microtubules (Figure 1a), the CMFs would have the

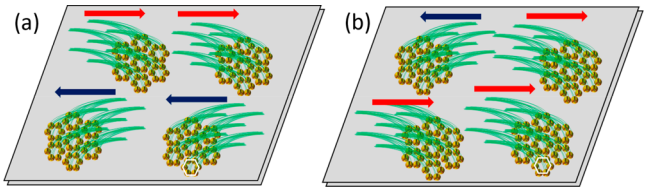

Figure 1. Schematic illustration of two possible movement directionalities of CSCs: (a) equal probability for two opposite directions along the microtubule axis and (b) preferential direction along one direction over the other. This image is drawn with the hexagonal arrays of rosette-shaped CSCs (marked with hexagon-shaped outlines) observed in electron microscopy imaging of the SCW of a unicellular green alga *Micrasterias*.[18] Cellulose chains extruded from each rosette-shaped CSCs are assembled into elementary CMFs which can be bundled into macrofibrils.

bidirectional packing, on average, along the MFA axis. However, it was recently reported that in the xylem cell wall induced in the epidermis of *Arabidopsis* hypocotyl, the CSC movements can be preferentially unidirectional (biased toward one direction of the cortical microtubule over the other direction, as shown in Figure 1b).[12] This would result in the partially unidirectional deposition of CMFs in the cell wall. The degree of unidirectionality or deviation from the bidirectionality of CMFs in SCWs will be directly related to the preferential CSC movement along one direction over the other during the cellulose synthesis in plant cell walls. Thus, if one can distinguish the unidirectional versus bidirectional deposition of the CMFs in the cell wall, it would be possible to infer the directionality of the CSC movement during the CMF synthesis and deposition.

Various analytical techniques have been employed for structural analyses of cellulose in plant cell walls; these include X-ray diffraction (XRD), X-ray or neutron scattering, nuclear magnetic resonance (NMR), and vibrational spectroscopy such as infrared (IR), Raman, and sum frequency generation (SFG). Diffraction and scattering techniques can reveal the recurring structural order of CMFs from subnanometer to mesoscale (1−100 nm),[19−23] but they cannot determine the directionality of CMFs. NMR can probe the molecular conformations of cellulose and dynamic interactions with other matrix polymers in plant cell walls,[24−27] but it cannot provide information on the directionality of CMFs. IR and Raman spectroscopy often suffer from spectral interferences from noncellulosic polymers copresent in plant cell walls.[28−31] In contrast, SFG is proven to be sensitive to crystalline cellulose only in the plant cell walls.[32−34] This cellulose specificity originates from the noncentrosymmetry requirement of the nonlinear optical process.[35−38] In the plant cell wall, the crystalline cellulose is the only component meeting this requirement and other amorphous polysaccharides cannot produce SFG signals.[32] In this paper, we demonstrate that the same noncentrosymmetry requirement can be combined with the SFG phase synchronization principle to determine the overall directionality of the CMFs in plant cell walls.

The proof of concept for this approach was originally suggested by recent time-dependent density functional theory (TD-DFT) calculations predicting SFG spectral features for uniaxially aligned cellulose crystallites in unidirectional and bidirectional packing.[39] Figure 2 schematically illustrates two cellulose crystals (represented with square rods) separated by a given distance, Δl, and the TD-DFT calculation results for the unidirectional and bidirectional packing cases with $\Delta l = 0$ (intimate contact). The transition dipole moments of the SFG-active OH stretch modes are in the (200) plane of the cellulose Iβ unit cell with specific tilt angles from the chain axis.[30,39,40] In contrast, the transition dipole moments of the SFG-active CH and CH_2 stretch modes are off the (200) plane. Thus, the OH dipoles can be enhanced when two crystallites are unidirectional (parallel) and canceled when the *c* axis is in the opposite direction for two crystals, making two crystallites bidirectional (antiparallel) to each other. In contrast, such cancellation effects for the same flipping are weaker for the CH dipoles. For

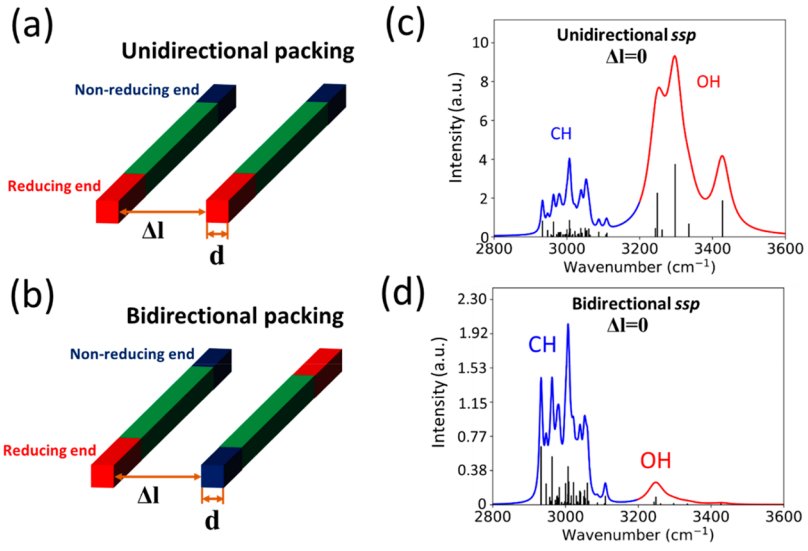

Figure 2. Schematic illustration of two cellulose crystallites in (a) unidirectional and (b) bidirectional packing, and TD-DFT prediction of SFG spectral features for two crystals in intimate contact with (c) unidirectional and (d) bidirectional packing. Calculations were for crystalline domains consisting of cellobiose units with atomic positions in the cellulose Iβ coordinate. Note that the *y* scale of the bidirectional packing case (d) is about 4 times smaller than the unidirectional case (c).[30,39]

https://dx.doi.org/10.1021/acs.jpcb.0c07076
J. Phys. Chem. B 2020, 124, 8071−8081

this reason, the OH SFG peak is predicted to be larger than the CH SFG peak for the unidirectional-packed crystals (Figure 2c) and smaller for the bidirectional-packed crystals (Figure 2d). Here, the degree of enhancement or cancellation effects depends on the degree of phase matching between SFG signals of adjacent crystallites which is in turn a function of the intercrystallite distance, Δl.

This paper explains how the phase synchronization function can be used to predict the SFG intensities of the CH and OH stretching modes of cellulose using the transition dipole moments determined from TD-DFT. The theoretical calculations in this paper are for the uniaxially aligned cellulose crystallites relevant to the CMFs in SCWs. Then we confirm the theoretical predictions for the bidirectional case using a well-controlled model system consisting of the cellulose nanocrystals (CNCs) suspended in D_2O at different concentrations and placed in a capillary tube. This model system provides equally spaced, uniaxially aligned CNCs without preferential directionality (so, equivalent to the bidirectional polarity in average). Finally, we employ the theoretically predicted OH/CH SFG intensity ratio to argue that CMFs in two xylem-type walls have unidirectional polarity, which is quite unexpected considering that the volume-averaged SFG signals of many SCW samples indicate that bidirectional CMFs are dominant.[41]

METHODS

Cellulose Nanocrystal Suspension Solutions. The tunicate mantle of tunicate (*Halocynthia roretzi*), kindly provided Okasei Ltd. (Onagawa, Japan), was used as starting material. After purification by alternating treatment by alkali and sodium chlorite, the samples were cut to strips about 2 mm wide and treated with a double-cylinder-type homogenizer in water. The resulting slurry was centrifuged to remove excess water and hydrolyzed in 50% sulfuric acid at 55 °C at a solid content of 1−2% for 20 h under continuous agitation using a PTFE-coated propeller. After removal of most of the sulfuric acid by centrifugation at 20 000*g*, the sample was repeatedly diluted and centrifuged at about 3000*g* for 20 min with the transparent supernatant discarded. After several cycles of the slow speed centrifugation wash, the supernatant starts to contain colloidal particles with a milky appearance. This supernatant was harvested by centrifugation at 20 000*g* for 1 h. This operation was repeated until no colloidal particle was left floating, leaving acid-resistant agglomerates in the slow centrifugation step. The colloidal particle was further washed with repeated centrifugation at 20 000*g* for 8 h and dilution with deionized water until the electric conductivity of the suspension was below 100 μS/cm. The counterion sulfate group was then exchanged to sodium by adding a dilute NaOH solution and sonicated at about 1% solid content using an ultrasonic homogenizer until the temperature of the water increased by about 20 °C. The water was exchanged to heavy water again by repeated centrifugation and dilution using 99.9% D_2O. The suspension at 4% was then kept as the stock solution and diluted with D_2O to prepare different concentrations.

***Arabidopsis* Hypocotyls.** We generated *Arabidopsis* transgenic plants expressing a master regulator of xylem differentiation, Vascular-related NAC-domain 7, fused to a glucocorticoid receptor (35S::VND7-GR).[12] *Arabidopsis* seeds were surface sterilized with 30% (v/v) bleach for 15 min, thoroughly washed with autoclaved double-distilled H_2O (ddH_2O), and stored at 4 °C for 3 days. Seeds of the homozygous transgenic line containing 35S::VND7-GR were grown in the dark for 3 days at 21 °C on vertical half-strength Murashige and Skoog (MS) plates containing 1% sucrose. Three-day-old *Arabidopsis* seedlings were transferred to microcentrifuge tubes containing liquid half-strength MS medium with 3% sucrose that was supplemented with either 20 μM dexamethasone (DEX) for induced samples or an equivalent volume of the solvent, dimethyl sulfoxide (DMSO), for control seedlings. Seedlings were treated with DEX or DMSO for 60 h and then collected for SFG analysis.

Celery Tracheary Elements. Celery tracheary elements were prepared as per the protocol published by D. G. Gray.[42] Vascular bundle strands (approximately 10−20 of roughly 10 cm in length) were stripped out of mature petioles, boiled in 1 L of water for 30 min, and then soaked for 1 h at room temperature in 1 L of a 5% w/v NaOH aqueous solution. Strands were then rinsed well and incubated for 1 h at 35 °C in 500 mL of an aqueous solution containing 40 g of $NaClO_2$ and 7.5 g of CH_3COOH. The bleached white strands were washed several times with a few liters of distilled water until the pH of the wash solution was stabilized. The prepared strands were stored moist under refrigeration.

Sum Frequency Generation Spectroscopy. Cellulose crystals are SFG active because of their noncentrosymmetric space group.[22,23] Thus, by temporal and spatial overlapping of two pulsed laser beams, 800 nm and IR, SFG signals can be generated. The 800 nm laser pulse was generated by a Ti-Sapphire amplifier (Coherent, Libra) at a 2 kHz repetition rate with an 85 fs pulse duration, 12 nm pulse width (full width at half-maximum), and 2.4 mJ pulse energy. For improving the spectral resolution, the pulse was narrowed using two Fabry−Perot etalons to 0.78 nm. The tunable IR was generated with an optical parametric amplifier/generator (OPA/OPG) system (Coherent, OPerA Solo). The broad-band IR laser pulses had 150−200 cm^{-1} fwhm, and it can scan from 1000 to 4000 cm^{-1}. The IR (5−12 mW) and 800 nm (8 mW) laser pulses were directed in parallel to a microscope (Olympus, BX51W1) entrance port and focused on a sample using a 36× reflective objective lens (NA = 0.52, Newport). The incident angle for 800 nm and IR pulse lens was 22.5° ± 7.5° from the opposite sides of the surface normal direction, and the irradiated area was about 4.1 μm × 2.4 μm.[33] The broad-band SFG signal then passes a monochromator, spectrally resolves using a volume-phase holographic grating, and is then collected by a CCD camera. The laser and microscope systems were discussed in detail by Lee et al.[43] and Huang et al.[33]

The control experiment with the CNC suspension solution was carried out with a table-top system in reflection mode.[43] The *Arabidopsis* and celery experiments were done with the microscopy system in a transmission mode with a 3 μm step scanning. Freshly prepared samples were put in D_2O overnight to replace water (H_2O) in the sample; this allowed probing the OH stretch bands in crystalline cellulose in the sample fully hydrated in D_2O.[16,33,34] Note that the OH/OD exchange can occur readily at the surface of the crystals, but the exchange for core OH groups is an extremely slow process at room temperature because D_2O hardly diffuses into the interior of the crystalline domain.[16,33,34] The samples were sandwiched between a slide glass and a coverslip and sealed using nail polish. The SFG signal was collected for the CH−CH_2 stretch region (2800−3000 cm^{-1}) and OH stretch region (3200−

https://dx.doi.org/10.1021/acs.jpcb.0c07076
J. Phys. Chem. B 2020, 124, 8071−8081

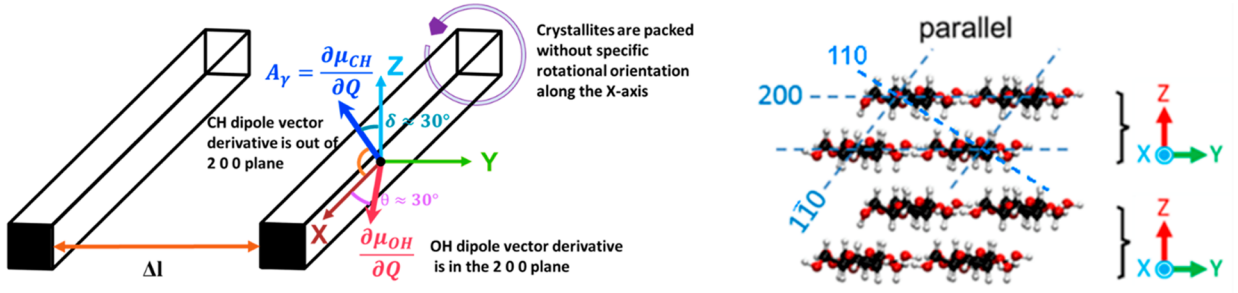

Figure 3. One-dimensional model for the theoretical calculation of the SFG intensity as a function of the interparticle separation distance (Δl). Image in the right shows eight chains of cellulose in the Iβ allomorph along the chain axis. When the (200) plane of cellulose Iβ is in the XY plane of the lab coordinate and the c axis is aligned to the X axis, the transition dipole moment of the CH stretch mode is assumed to be tilted by 60° from the X axis toward the Z axis (away from the (200) plane; thus, $\delta \approx 30°$). Transition dipole moment of the OH stretch mode is tilted by 30° from the chain axis toward the Y axis (within the (200) plane). These angles are chosen for the simulation based on the TD-DFT calculations and the polarization IR measurements.[30,39,40] Right image is copied from ref 39 with permission conveyed from Copyright Clearance Center Inc.

3500 cm^{-1}), and hyperspectral imaging processing was done using Mathematica.[33]

THEORETICAL CALCULATIONS

The dependence of the SFG intensity of the uniaxially aligned CMFs on the directionality (unidirectional vs bidirectional) and the distance between CMFs can be modeled using nonlinear optical theory summing the SFG signals from polycrystalline domains taking into account randomizing phase distribution terms[44]

$$I_3 \propto I_2 I_1 \left| \sum_{m=1}^{q} \chi_m^{(2)} \frac{e^{-i\Delta k l_m} - 1}{\Delta k} e^{-i\Delta k \sum_{j=1}^{m-1} l_j} \right|^2 n^2 \quad (1)$$

$$\chi_m^{(2)} \propto M_{\alpha\beta} A_\gamma \quad (2)$$

$$\Delta k = k_1 + k_2 - k_3,\ k_i = \frac{n_i \omega_i}{c} \quad (3)$$

$$L_c = \frac{2}{\Delta k} \quad (4)$$

Here, I_3, I_2, and I_1 are the intensities of the SFG signal, the 800 nm upconversion beam, and the resonant IR beam, respectively, $\chi_m^{(2)}$ is an effective second-order susceptibility tensor of the SFG-active vibrational mode of the mth crystal which is the product of the Raman ($M_{\alpha\beta}$) and the IR (A_γ) transition moments of the crystal at given polarization combinations of SFG, 800 nm, and IR beams, l_m and l_i are the dimension of each domain contributing to the overall SFG, and Δk is the phase mismatch between the SFG signal (k_3) and the sum of the input wave vectors of IR (k_1) and 800 nm (k_2), which can be calculated from the refractive index (n_i) of the medium, the speed of light (c), and the angular frequency (ω_i) of each beam. The magnitude of Δk determines the coherence length (L_c) beyond which the SFG yield becomes insignificant.[37,38] In eq 1, the $\frac{e^{-i\Delta k l_m} - 1}{\Delta k}$ term represents the effect of wave vector mismatch on the SFG intensity of the mth domain and the $e^{-i\Delta k \sum_{j=1}^{m-1} l_j}$ term represents the phase randomization effect on the SFG intensity by neighboring domains with different sizes (l_j) or orientations in a polycrystalline medium.[44]

To theoretically explain the difference in SFG intensity dependence on the interparticle distance (Δl) for the unidirectional and bidirectional CMFs (Figures 2a and 2b), a simplified one-dimensional model system will be considered. In this simplified model (Figure 3), all cellulose crystals are assumed to have the same diameter (d) and the crystal c axis (chain axis) is aligned along the X axis in the lab coordinate. The crystals are assumed to have the full 360° rotational degree of freedom along the alignment axis;[45] if there are some degrees of registry between certain crystallographic facets of CMF in cell walls, this assumption can be modified. The tilt angles of the transition dipole moments ($\partial\mu/\partial Q$) of the CH and OH stretch modes are shown in Figure 3 based on the previous theoretical calculations and polarization-IR measurements.[30,39,40] For simplicity of the calculation, the $\chi_m^{(2)}$ orientation will be assumed to be the same as the IR tensor orientation. The previous TD-DFT calculations showed that for the cases of unidirectional and bidirectional packing of crystals, the Raman transition is not significantly different between the two cases;[39] so, it would not affect the model calculation result significantly. The $\chi_m^{(2)}$ term is a positive value when the chain direction is unidirectional and can be positive or negative depending on the directionality along the X axis when CMFs are bidirectional.

In this model, the domain size (l_m) can be assumed to be either the diameter of the cellulose crystal (d) or the distance between the crystals (Δl), and these two domains appear alternatively along the Y direction in Figure 3. Thus, in eq 1, odd m's are cellulose crystals ($\chi_{odd}^{(2)} \neq 0$; ± depending on the chain directionality along the X axis) and even m's are amorphous domains ($\chi_{even}^{(2)} = 0$) ($\chi_{even}^{(2)} = 0$). It also simplifies the summation term of the exponent in the phase randomization factor to $\sum_{j=1}^{m-1} l_j = \left\lceil \frac{m-1}{2} \right\rceil d + \left\lfloor \frac{m-1}{2} \right\rfloor \Delta l$. Then eq 1 for the unidirectional and bidirectional packing of cellulose crystals can be converted to eqs 5 and 6, respectively

$$I_3 \propto \left| \sum_{f=1}^{n-1} I_2 I_1 e^{-f(d+\Delta l)} \chi_1^{(2)} d^2 \frac{e^{-i\Delta k d} - 1}{\Delta k} (e^{-i\Delta k (d+\Delta l) f}) n^2 (\cos\theta + \cos\delta \sin\theta) \right|^2 \quad (5)$$

https://dx.doi.org/10.1021/acs.jpcb.0c07076
J. Phys. Chem. B 2020, 124, 8071−8081

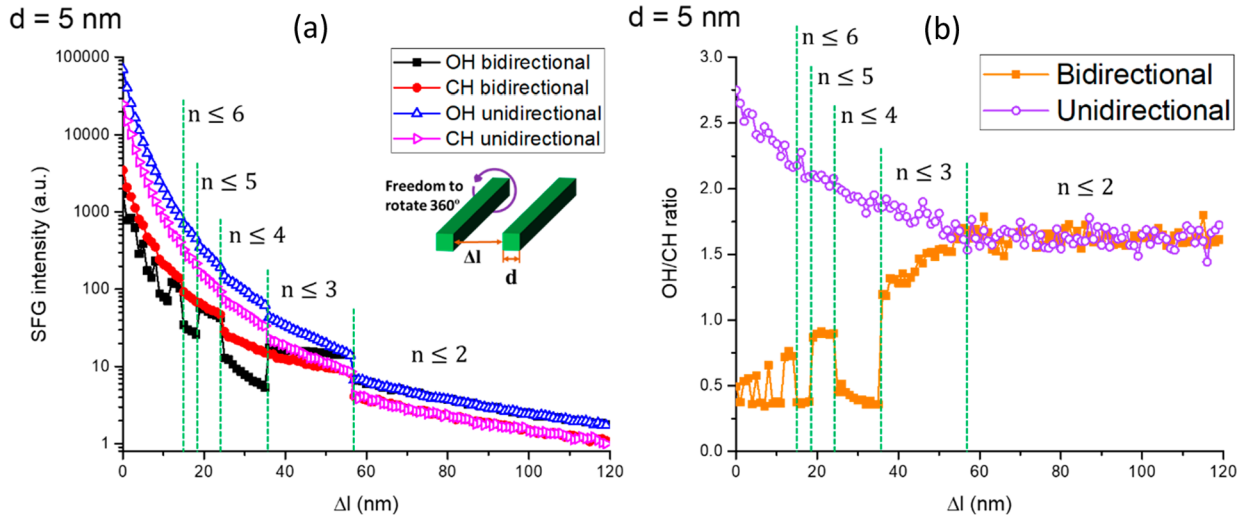

Figure 4. (a) Theoretical prediction of the CH and OH stretch modes for the unidirectional (open symbols) and bidirectional (filled symbols) packing of cellulose crystals (modeled in Figure 3) as a function of Δl. Here, n indicates the number of crystals within the SFG coherence length (L_c) and the diameter of each crystal (d) is 5 nm. (b) Theoretically calculated OH/CH intensity ratio for the unidirectional and bidirectional uniaxial packing of cellulose crystals as a function of Δl. Each data point is the average of calculation results for 1000 orientations of the (200) plane created with a random function generator.

$$I_3 \propto \left| \sum_{f=1}^{n-1} I_2 I_1 e^{-f(d+\Delta l)} \chi_1^{(2)} d^2 \frac{e^{-i\Delta k d} - 1}{\Delta k} (e^{-i\Delta k (d+\Delta l) f}) n^2 \right.$$
$$\left. ((-1)^f (\cos\theta) + \cos\delta \sin\theta) \right|^2 \quad (6)$$

where θ is the polar angle of the transition dipole vector from the X axis, δ is the tilt angle between the transition dipole vector from the Z axis, and n is the number of crystals within the coherence length along the Y direction, $n = L_c/(d + \Delta l)$.

Note that eqs 5 and 6 are the simplified versions of eq 1, showcasing the hypothetical condition of the perfectly unidirectional and alternatively bidirectional packings of the uniaxially aligned crystals of the same size with an identical separation distance in one dimension. These equations do not replicate the exact situation of CMFs in plant cell walls which are deviating from the ideal case shown in Figure 3. However, the solutions of these equations can provide the physical insights needed to determine the CMF directionality from the SFG spectra of plant cell walls. The full Mathematica program solving these equations numerically with the random distribution of crystal orientation around the X axis is provided in the Supporting Information.

It should be noted that the physical system considered here is different from the phase-sensitive SFG or second-harmonic generation (SHG) used to determine the average or net polarity of molecules at two-dimensional (2D) interfaces. In the phase-sensitive detection method, the signals from the interfacial molecules (which are all within the coherence length) are mixed with an externally generated reference signal with a known phase at the same frequency of SFG or SHG signal; then the net polarity (i.e., "pointing up" vs "pointing down") of molecules with respect to the 2D plane is determined.[46−49] This existing phase-sensitive detection method would be difficult to apply to crystalline cellulose interspersed three dimensionally in an amorphous matrix because the SFG signal comes from the entire probe volume that is often larger than the coherence length dimension. A digital holographic imaging could extract the intensity and phase information over an extended depth of focus,[50] but it requires scanning one wavelength at a time and has not been demonstrated for the broad-band SFG. On the basis of the theoretical model discussed here, one can determine the "relative phase" of SFG-active domains within the coherence length if there are two peaks that have different symmetry cancellation efficiency. In the case of CMFs, the symmetry cancellation effects of the CH and OH signal are found to be different upon parallel (unidirectional) vs antiparallel (bidirectional) packing.[39,51] The theoretical consideration presented here cannot determine the "absolute phase" of CMFs with respect to the lab frame because the external reference beam is not used.

RESULTS AND DISCUSSION

Theoretical Prediction for Unidirectional vs Bidirectional Packing in One Dimension. Figure 4a plots the SFG intensities calculated for the CH and OH stretch modes of uniaxially aligned cellulose crystals with d = 5 nm as a function of Δl for the unidirectional (eq 5) and bidirectional (eq 6) packing. This crystal diameter is chosen because the CMFs in plant cell walls are typically 3−5 nm in diameter.[52] A case with d = 20 nm is shown in the Supporting Information for comparison. In this calculation, the SFG coherence (L_c) is set as 120 nm, which is the value calculated for our experimental reflection geometry.[41,43]

For the unidirectional packing case, both CH and OH SFG intensities increase monotonically as Δl decreases, which is the consequence of the increase in the cellulose concentration within L_c. In our simple one-dimensional model, n increases in integer; so, there is a sudden jump whenever n changes. This is just an artifact of the simplified one-dimensional model. In reality, the SFG intensity will vary smoothly as the cellulose concentration increases in the sample, because of local variances in inter-CMF distances and CMF angles within the probing volume.

https://dx.doi.org/10.1021/acs.jpcb.0c07076
J. Phys. Chem. B 2020, 124, 8071−8081

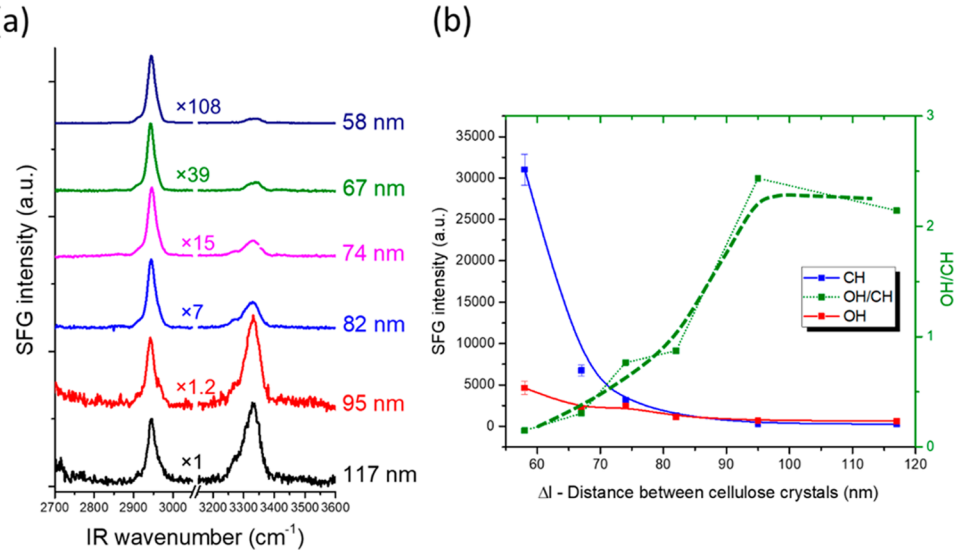

Figure 5. (a) SFG spectra of uniaxially aligned CNCs dispersed in D_2O in a rectangular capillary tube. Alignment direction is along the capillary tube.[58] SFG spectra were collected in the reflection geometry with the *ssp* polarization; number next to each spectrum is the relative intensity of the CH peak used for normalization of the spectrum for comparison. Interparticle distance was calculated from the CNC concentration (see the Supporting Information). Directionality of CNCs in the suspension is random along the alignment axis; thus, it is equivalent to the bidirectional packing on average over the coherence length scale. (b) Plots of CH and OH SFG areas (in the left *y* scale) and the OH/CH ratio (in the right *y* axis). Cellulose crystals extracted from tunicate were dispersed in D_2O, where they form hexagonal arrays all aligned along the capillary tube.

In the case of bidirectional packing, the OH SFG intensity increases as Δl decreases within the same n range but significantly drops when n varies from odd numbers to even numbers (for example, $n \leq 3 \rightarrow n \leq 4$). This is because the symmetry cancellation effect of the OH transition dipoles pointing toward the opposite directions is larger than the concentration increase effect (n^2 in eq 6) at that specific Δl region. In contrast, the symmetry cancellation effect is relatively insignificant for the CH transition dipoles; thus, the SFG intensity drop is negligible at the change of n from odd numbers to even numbers.

Figure 4b compares the ratio of the calculated SFG intensities of the OH and CH stretch modes for the uniaxially aligned cellulose crystals with the unidirectional versus bidirectional packing. In the unidirectional packing, the OH/CH ratio increases monotonically from the fully isolated case ($\Delta l \geq L_c$) to the intimate contact case ($\Delta l = 0$). In contrast, the OH/CH ratio of the bidirectional packing decreases from the fully isolated case in a nonmonotonic and sinusoidal way with decreasing periodicity as Δl decreases from L_c to zero.

The calculation result for the simple one-dimensional model suggests that if one can estimate the inter-CMF distance (Δl) from the volumetric concentration of cellulose in the sample and knows that CMFs are aligned uniaxially along the main MFA axis from X-ray diffraction,[4,17] then the average directionality of the CMFs in the sample can be determined by measuring the OH/CH intensity ratio of cellulose in SFG (Figure 4b). Note that the theoretical calculation predicting the SFG OH/CH intensity ratio of CMFs in the real sample is extremely difficult and much more complicated because the angle and separation distance of CMFs vary locally within the sample.[12,53,54]

The data in Figure 4a also suggest that the CH SFG intensities of different samples (for example, at different growth stages) can be used to compare the relative concentration of CMFs in the samples as long as the CMF packing pattern and directionality do not change between samples.[55,56] However, the OH SFG intensity cannot be used for such purposes when CMFs are packed bidirectionally.[51] The quantitative comparison of the absolute intensity in experimental data with the calculation result is not possible because of complications from local structural variations and scattering of the light in opaque plant cell walls. However, these complications do not matter in the case of the directionality study since the CH SFG intensity is used as an internal standard to normalize the OH SFG intensity (Figure 4b).

Verification of Theoretical Prediction for Uniaxial Packing without Preferential Directionality. There are many ways to prepare the uniaxially aligned CNC samples; such methods include mechanical stretching of a polymer matrix in which CNCs are interspersed,[51] shear-assisted deposition of CNCs into thin films,[22] and suspension of CNCs in a capillary tube filled with water with extremely low ionic strength. In all these methods, it is thermodynamically difficult (if not impossible) to align CNCs with unidirectional polarity. The random directionality along the alignment axis is entropically favorable, which is equivalent to the bidirectional packing on average over the space. Among these methods, we chose the CNC suspension method because small-angle X-ray diffraction (SAXS) analysis showed that the CNCs suspended in pure water form a hexagonally packed array with a constant interparticle distance.[57] Due to the viscosity increase at high CNC concentrations, the practical upper limit of the CNC concentration was ~4 wt % to use the capillary method. Using a simple geometry argument, the interparticle distance (Δl) is calculated to be ~58 nm at 4 wt % (see the Supporting Information). By diluting this solution, a series of uniaxially aligned CNCs with bidirectional packing and varying Δl could be prepared.

The SFG spectra of the uniaxially aligned and bidirectional CNCs with interparticle distances (Δl) varying from ~58 to ~117 nm are shown in Figure 5a. In the reflection-SFG geometry used in this experiment, the coherence length (L_c) is

https://dx.doi.org/10.1021/acs.jpcb.0c07076
J. Phys. Chem. B 2020, 124, 8071−8081

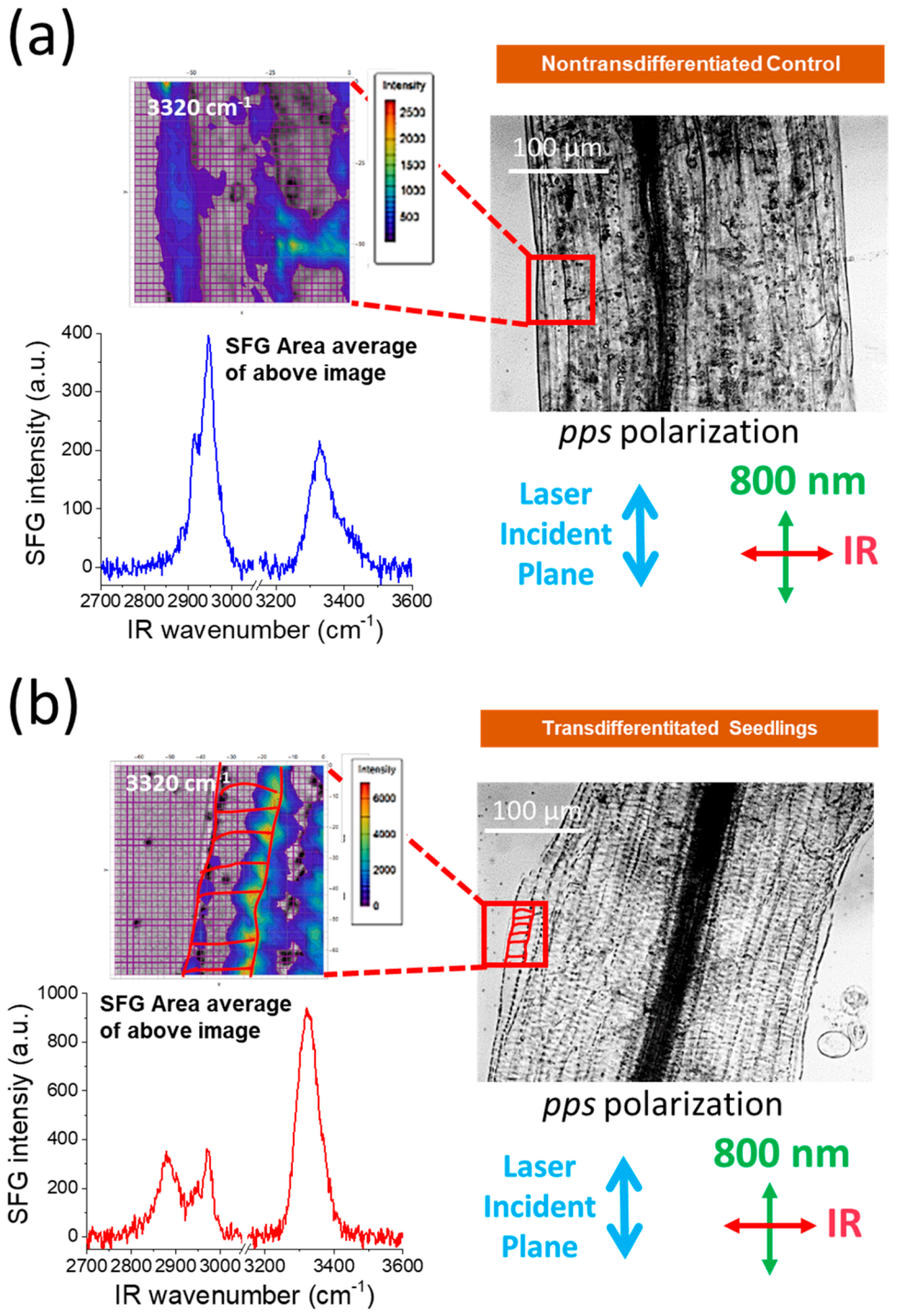

Figure 6. Microscopic SFG analysis of (a) nontransdifferentiated and (b) transdifferentiated epidermis of *Arabidopsis* hypocotyl never dried and fully hydrated in D_2O. Optical image of each sample is shown with the scale bar (100 μm). Area of 70 μm × 70 μm (marked with a box) was analyzed with a 2 μm step interval. Broad-band SFG spectra were collected in the CH and OH regions at each image pixel; SFG intensity at 3320 cm^{-1} is shown in the 2D map. Full spectra of the CH and OH regions shown here are constructed by taking the area average of the raw SFG data from each pixel.

calculated to be ~120 nm (Supporting Information, Mathematica code). The OH and CH SFG peak areas as well as their ratios are plotted in Figure 5b. As predicted in Figure 4a for the bidirectional packing, both OH and CH intensities increase as Δl decreases, but the CH intensity becomes larger than the OH intensity at short Δl distances. Since $L_c \approx 120$ nm, the OH/CH ratio at $\Delta l \approx 117$ nm can be assumed to be the ratio of intrinsic $\chi^{(2)}_{OH}$ and $\chi^{(2)}_{CH}$ values without interparticle interferences. When $\Delta l > L_c$, the intensity of SFG is not influenced by the dipole cancellation. Thus, the relative SFG intensities can be directly related to the relative magnitudes of the second-order susceptibility tensors (eq 2) of the OH and CH stretch modes. As Δl decreases below L_c, the OH/CH ratio decreases as predicted in Figure 4b for the bidirectional packing. Although the sinusoidal variance (Figure 5b) is not as clear as the prediction from the simple one-

https://dx.doi.org/10.1021/acs.jpcb.0c07076
J. Phys. Chem. B 2020, 124, 8071−8081

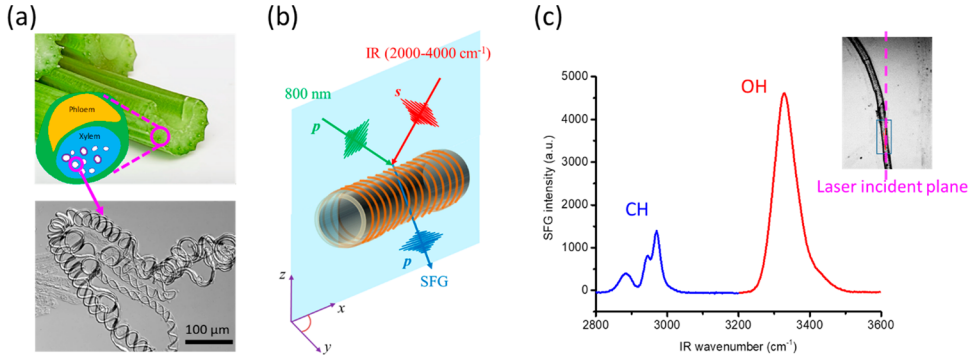

Figure 7. (a) Optical image of the celery cross-section and microscopic image of cellulose macrofibril coils isolated from the tracheary elements. (b) Experimental geometry of the transmission-SFG measurement. Coil axis is placed in the laser incidence plane, and SFG polarization combination is *pps*; thus, IR polarization is nearly parallel to individual cellulose microfibrils. (c) SFG spectrum of the cellulose macrofibril coil aligned along the laser incidence plane. SFG spectrum of the coil aligned perpendicular to the laser incidence plane is shown in Figure S3.

dimensional model (Figure 4a), the experimentally observed trend is qualitatively consistent with the symmetry cancellation effect considered in the theoretical calculation for the uniaxial packing with the bidirectional packing.

Evidence for the Unidirectional Packing of CMFs in SCW of Transdifferentiated Xylem Cells. In the previous volume-averaged SFG analysis of SCWs of land plants, the OH SFG intensity of cellulose was found to be much smaller than the CH SFG intensity.[41] This was interpreted as the majority of CMFs in the land plants with thickened SCWs are effectively bidirectional to each other. However, live-cell imaging of fluorescent protein-tagged CSCs during SCW formation in transdifferentiated xylem cells suggested that the CSC movements are not bidirectional with the equal probability of moving toward the opposite directions along the microtubule.[12] If so, the CMFs in those cell walls will not be fully bidirectional; they will have some degree of unidirectionality. Thus, this system was chosen for the directionality study with SFG.

Figure 6 shows the SFG analysis results for nontransdifferentiated and transdifferentiated cells of the *Arabidopsis* hypocotyl. The hoop-shaped cell walls can be recognized in Figure 6b, indicating that the DEX treatment successfully induced transdifferentiation of epidermal cells of *Arabidopsis* hypocotyls into xylem vessel elements.[12] The SFG mapping of the 3320 cm^{-1} peak shows stronger intensities near the cell boundaries because a larger amount of the cell wall was projected to the image plane at that location. The cellulose-containing wall exists only at the external surface of each cell which is larger than the SFG probe depth of this experiment. Our SFG microscope system has an effective probe depth (depth of focus) larger than 10 μm. Thus, the vertical regions of the cell wall at the cell boundaries fill a larger fraction of the probe volume than the horizontal walls in the top and bottom regions of the cell. In the area-averaged SFG spectrum of the nontransdifferentiated control, the CH peak at 2944 cm^{-1} is stronger than the OH peak at 3320 cm^{-1} (Figure 6a). In contrast, the SCWs in transdifferentiated xylem cells show the OH SFG intensity to be much stronger than the CH SFG intensity (Figure 6b) (also, see Figure S2). This high OH/CH SFG intensity ratio supports the fact that the CMFs in SCWs of transdifferentiated xylem cells are not entirely bidirectional; they must have some degree of unidirectionality, which is congruent with the biased unidirectionality found in the CSC movement tracking for the same sample.[12]

It is reasonable to expect that the cellulose content is higher in transdifferentiated xylem cells than that in nontransdifferentiated control; however, this cannot be responsible for the OH/CH intensity ratio difference between the control and the transdifferentiated xylem cells. If the CMFs were effectively bidirectional in SCWs of transdifferentiated cells, then the OH/CH intensity ratio would have been lower than the nontransdifferentiated cells because of the larger symmetry cancellation effect for the higher cellulose concentration sample (thus, smaller Δl in Figures 4b and 5b). That is the opposite to the experimental observation. Thus, the high OH/CH SFG intensity ratio must be due to the "net" unidirectional packing of CMFs in the transdifferentiated xylem cells.

It is important to note that the OH/CH ratio in biological tissues can vary by multiple factors. The change in the orientation of microfibrils can impact the OH/CH ratio as the microfibril relative position with respect to the laser incidence plane can vary depending on the analyzed location. The bundling of microfibrils can also affect the OH/CH ratio. The OH/CH ratios can also be affected by the existence of noncellulosic compounds in the probing area which can absorb the IR beam in one region (CH or OH) more than the other. Investigation of all of these possibilities is beyond the scope of this study.

Cellulose coils in tracheary elements of celery can be isolated,[42] which make them an ideal sample for SFG analysis of the CMF directionality (polar ordering) without contributions of SFG signals from other types of cell walls. Figure 7a shows the optical microscope image of the cellulose macrofibrils isolated from celery treachery coils. Their diameter is about 2−3 μm. Sugar analysis of the celery treachery element indicated that the cellulose content is ∼75%,[42] which would correspond to an inter-CMF distance of ∼4 nm (side to side) assuming the full dispersion of individual 4 nm thick CMFs in the sample. Using the transmission geometry of the SFG measurement sketched in Figure 7b, the coherence length is estimated to be ∼6.3 μm; thus, $\Delta l/L_c \approx 0.0003$. This sample gives an OH/CH intensity ratio of ∼5, which is significantly larger than the intrinsic $\chi^{(2)}_{OH}/\chi^{(2)}_{CH}$ ratio (∼2.3 in Figure 5b) of cellulose Iβ estimated from the $\Delta l \approx L_c$ case. In the one-dimensional model calculation for the unidirectional packing (Figure 4b), the OH/CH intensity ratio is predicted to increase almost by a factor of 2 as $\Delta l/L_c$ approaches zero compared to the $\Delta l/L_c = 1$ case. The preferential orientation of the CMFs with respect to the laser incidence plane cannot

https://dx.doi.org/10.1021/acs.jpcb.0c07076
J. Phys. Chem. B 2020, 124, 8071−8081

explain this large OH/CH ratio (Figure S3). Comparison of the experimental value (Figures 6c and S3) with this theoretical prediction (Figure 4b) suggests that the elementary CMFs in the celery tracheary element coil must have a high degree of unidirectional polarity.

One may question whether the chirality of cellulose may influence the OH/CH intensity ratio upon switching the directionality from the parallel (unidirectionally biased) to antiparallel (bidirectional) packing. The SFG of cellulose does not follow the conventional achiral/chiral rule of the SFG of the 2D surface with C_∞ symmetry. Figure S4 compares the SFG spectra collected with different polarization combinations known to be sensitive to chiral and achiral molecules for a reference sample created by uniaxial packing of cellulose Iβ crystals isolated from tunicate. Since the uniaxial packing was induced during solution evaporation with a shear force,[22] there is no preferential directionality of the cellulose crystals along the preferential packing axis. In Figure S4, the *ppp*-SFG spectrum of cellulose crystals aligned along the laser incidence plane is almost identical to the *sss*-SFG spectrum of cellulose aligned perpendicular to the laser incidence plane. Similarly, the *pps* spectrum for the in-plane orientation is very similar to the *ssp* spectrum of the out-of-plane orientation and so on. This means that the SFG spectral features of cellulose are more sensitive to the azimuth angle dependence than the chiral/achiral polarization combination. Still the azimuth angle dependence alone (Figure S4) cannot explain the OH/CH intensity ratio larger than 2 for the uniaxially aligned CMFs.

The data shown in Figures 6 and 7 imply that CMFs in xylem or xylem-like cells in other plants may have unidirectional packing. This is in stark contrast to the fully developed cotton fibers, which give a OH/CH ratio of ~0.2,[56] indicating almost perfect bidirectional packing. These experimental observations raise a few important questions that have not been asked or systematically studied in plant biology. What controls the directionality (or polarity) of the CSC movement during the cellulose synthesis? How is the CMF directionality associated with the biological and mechanical functions of the cell at the specific growth stage of the plant? The theoretical foundation and experimental confirmation reported in this paper open an unprecedented opportunity to study these questions related to the cellulose biosynthesis with SFG. The same principle and methodology can also be applied to other crystalline biopolymers such as chitin, amylose, collagen, etc., that are SFG active due to their noncentrosymmetric crystal structures.[59−61]

CONCLUSIONS

In this study, theoretical calculations were combined with experiments to demonstrate the sensitivity of SFG to the nano/mesoscale arrangement of cellulose crystals in amorphous matrices. The transition dipole moments of cellulose and the phase synchronization principle of SFG were incorporated in the theoretical calculation for a simplified one-dimensional model to study the effect of crystal polarity and intercrystallite distance on the SFG intensity. From the calculations, the ratio of the SFG peaks in the OH and CH stretch regions (OH/CH) was found to be highly dependent on the polar order (unidirectional vs bidirectional) of uniaxially aligned cellulose crystals and the distance between the crystals. The OH/CH ratio increases for the unidirectional-packing case and decreases for the bidirectional-packing case as the distance between crystals decreases. As the intercrystal distance increases to the SFG coherence length, the OH/CH ratios of both cases converge to the intrinsic value of isolated crystals without spectral interference with each other. The theoretical prediction for the bidirectional packing of cellulose crystals was confirmed experimentally. On the basis of the theoretically predicted and experimentally proven trends, it was found for the first time that the induced xylem cells of *Arabidopsis* and celery tracheary elements have a biased unidirectional packing of cellulose microfibrils in the cell wall.

ASSOCIATED CONTENT

Supporting Information

The Supporting Information is available free of charge at https://pubs.acs.org/doi/10.1021/acs.jpcb.0c07076.

Calculation of the distance between crystals with a hexagonal lateral packing; SFG intensity calculations for CH and OH stretch modes for 20 nm width crystals as a function of intercrystallite distance; control experiments for xylem-induced hypocotyls; SFG analysis for rotation of celery coils by 90° with respect to the laser incident plane; polarization dependence of the SFG signal for uniaxially aligned cellulose crystals; Mathematica code to calculate the SFG intensity of CH and OH stretch modes for unidirectional and bidirectional packing of crystals (PDF)

AUTHOR INFORMATION

Corresponding Author

Seong H. Kim − *Department of Chemical Engineering, Materials Research Institute, Pennsylvania State University, University Park, Pennsylvania 16802, United States;* orcid.org/0000-0002-8575-7269; Email: shkim@engr.psu.edu, shk10@psu.edu

Authors

Mohamadamin Makarem − *Department of Chemical Engineering, Materials Research Institute, Pennsylvania State University, University Park, Pennsylvania 16802, United States;* orcid.org/0000-0001-5559-8618

Yoshiharu Nishiyama − *University Grenoble Alpes, CNRS, CERMAV, Grenoble 38000, France;* orcid.org/0000-0003-4069-2307

Xiaoran Xin − *Department of Biochemistry and Molecular Biology, Pennsylvania State University, University Park, Pennsylvania 16802, United States*

Daniel M. Durachko − *Department of Biology, Pennsylvania State University, University Park, Pennsylvania 16802, United States*

Ying Gu − *Department of Biochemistry and Molecular Biology, Pennsylvania State University, University Park, Pennsylvania 16802, United States*

Daniel J. Cosgrove − *Department of Biology, Pennsylvania State University, University Park, Pennsylvania 16802, United States;* orcid.org/0000-0002-4020-5786

Complete contact information is available at: https://pubs.acs.org/10.1021/acs.jpcb.0c07076

Notes

The authors declare no competing financial interest.

https://dx.doi.org/10.1021/acs.jpcb.0c07076
J. Phys. Chem. B 2020, 124, 8071−8081

■ ACKNOWLEDGMENTS

The theoretical calculations and verification with uniaxially aligned CNC suspensions were conducted with the support by the Center for Lignocellulose Structure and Formation, Energy Frontier Research Center, funded by the U.S. Department of Energy, Office of Science, Basic Energy Sciences, under Award Number DE-SC0001090. The study on the transdifferentiated xylem cells of *Arabidopsis* and tracheary cellulose coils of celery was carried out as part of the iSuperSEED program of the Penn State MRSEC funded by the National Science Foundation (grant no. DMR-1420620). We are also thankful to the ESRF for allocating us beamtime at D2AM.

■ REFERENCES

(1) Albersheim, P.; Darvill, A.; Roberts, K.; Sederoff, R.; Staehelin, A. *Plant cell walls*; Garland Science, Taylor & Francise Group: New York, 2010.
(2) Cosgrove, D. J. Growth of the plant cell wall. *Nat. Rev. Mol. Cell Biol.* **2005**, *6* (11), 850−61.
(3) Bergfeld, R.; Speth, V.; Schopfer, P. Reorientation of Microfibrils and Microtubules at the Outer Epidermal Wall of Maize Coleoptiles During Auxin-Mediated Growth. *Bot. Acta* **1988**, *101* (1), 57−67.
(4) Reiterer, A.; Lichtenegger, H.; Tschegg, S.; Fratzl, P. Experimental evidence for a mechanical function of the cellulose microfibril angle in wood cell walls. *Philos. Mag. A* **1999**, *79* (9), 2173−2184.
(5) Zhong, R.; Burk, D. H.; Morrison, W. H.; Ye, Z.-H. A Kinesin-Like Protein Is Essential for Oriented Deposition of Cellulose Microfibrils and Cell Wall Strength. *Plant Cell* **2002**, *14* (12), 3101.
(6) Burk, D. H.; Ye, Z.-H. Alteration of Oriented Deposition of Cellulose Microfibrils by Mutation of a Katanin-Like Microtubule-Severing Protein. *Plant Cell* **2002**, *14* (9), 2145.
(7) Arantes, V.; Saddler, J. N. Access to cellulose limits the efficiency of enzymatic hydrolysis: the role of amorphogenesis. *Biotechnol. Biofuels* **2010**, *3* (1), 4.
(8) Chundawat, S. P. S.; Beckham, G. T.; Himmel, M. E.; Dale, B. E. Deconstruction of Lignocellulosic Biomass to Fuels and Chemicals. *Annu. Rev. Chem. Biomol. Eng.* **2011**, *2* (1), 121−145.
(9) Zhang, Y. H. P. Reviving the carbohydrate economy via multi-product lignocellulose biorefineries. *J. Ind. Microbiol. Biotechnol.* **2008**, *35* (5), 367−375.
(10) Donaldson, L. Cellulose microfibril aggregates and their size variation with cell wall type. *Wood Sci. Technol.* **2007**, *41* (5), 443.
(11) Anderson, C. T.; Carroll, A.; Akhmetova, L.; Somerville, C. Real-time imaging of cellulose reorientation during cell wall expansion in Arabidopsis roots. *Plant Physiol.* **2010**, *152* (2), 787−796.
(12) Li, S.; Bashline, L.; Zheng, Y.; Xin, X.; Huang, S.; Kong, Z.; Kim, S. H.; Cosgrove, D. J.; Gu, Y. Cellulose synthase complexes act in a concerted fashion to synthesize highly aggregated cellulose in secondary cell walls of plants. *Proc. Natl. Acad. Sci. U. S. A.* **2016**, *113*, 11348−11353.
(13) Zheng, Y.; Cosgrove, D. J.; Ning, G. High-resolution field emission scanning electron microscopy (FESEM) imaging of cellulose microfibril organization in plant primary cell walls. *Microsc. Microanal.* **2017**, *23* (5), 1048−1054.
(14) Xu, P.; Donaldson, L. A.; Gergely, Z. R.; Staehelin, L. A. Dual-axis electron tomography: a new approach for investigating the spatial organization of wood cellulose microfibrils. *Wood Sci. Technol.* **2007**, *41* (2), 101.
(15) Reza, M.; Ruokolainen, J.; Vuorinen, T. Out-of-plane orientation of cellulose elementary fibrils on spruce tracheid wall based on imaging with high-resolution transmission electron microscopy. *Planta* **2014**, *240* (3), 565−573.
(16) Huang, S.; Kiemle, S. N.; Makarem, M.; Kim, S. H. Correlation between crystalline cellulose structure and cellulose synthase complex shape: a spectroscopic study with unicellular freshwater alga Micrasterias. *Cellulose* **2020**, *27* (1), 57−69.
(17) Barnett, J. R.; Bonham, V. A. Cellulose microfibril angle in the cell wall of wood fibres. *Biol. Rev.* **1999**, *79* (2), 461−472.
(18) Giddings, T. H., Jr.; Brower, D. L.; Staehelin, L. A. Visualization of particle complexes in the plasma membrane of Micrasterias denticulata associated with the formation of cellulose fibrils in primary and secondary cell walls. *J. Cell Biol.* **1980**, *84* (2), 327−339.
(19) Newman, R. H.; Hill, S. J.; Harris, P. J. Wide-angle x-ray scattering and solid-state nuclear magnetic resonance data combined to test models for cellulose microfibrils in mung bean cell walls. *Plant Physiol.* **2013**, *163* (4), 1558−1567.
(20) Saxe, F.; Eder, M.; Benecke, G.; Aichmayer, B.; Fratzl, P.; Burgert, I.; Rüggeberg, M. Measuring the distribution of cellulose microfibril angles in primary cell walls by small angle X-ray scattering. *Plant Methods* **2014**, *10* (1), 25.
(21) Ye, D.; Kiemle, S. N.; Rongpipi, S.; Wang, X.; Wang, C.; Cosgrove, D. J.; Gomez, E. W.; Gomez, E. D. Resonant soft X-ray scattering reveals cellulose microfibril spacing in plant primary cell walls. *Sci. Rep.* **2018**, *8* (1), 12449.
(22) Nishiyama, Y.; Langan, P.; Chanzy, H. Crystal structure and hydrogen-bonding system in cellulose Iβ from synchrotron X-ray and neutron fiber diffraction. *J. Am. Chem. Soc.* **2002**, *124* (31), 9074−9082.
(23) Nishiyama, Y.; Sugiyama, J.; Chanzy, H.; Langan, P. Crystal structure and hydrogen bonding system in cellulose Iα from synchrotron X-ray and neutron fiber diffraction. *J. Am. Chem. Soc.* **2003**, *125* (47), 14300−14306.
(24) Atalla, R. H.; Vanderhart, D. L. Studies on the structure of cellulose using Raman spectroscopy and solid state C NMR. *Cellulose and wood-chemistry and technology*; Wiley: New York, 1988; pp 169−188.
(25) Horii, F.; Hirai, A.; Kitamaru, R. Solid-state 13 C-NMR study of conformations of oligosaccharides and cellulose. *Polym. Bull.* **1983**, *10* (7−8), 357−361.
(26) Wang, T.; Hong, M. Solid-state NMR investigations of cellulose structure and interactions with matrix polysaccharides in plant primary cell walls. *J. Exp. Bot.* **2016**, *67* (2), 503−514.
(27) Wang, T.; Park, Y. B.; Cosgrove, D. J.; Hong, M. Cellulose-pectin spatial contacts are inherent to never-dried Arabidopsis thaliana primary cell walls: evidence from solid-state NMR. *Plant Physiol.* **2015**, *168*, 871−884.
(28) Blackwell, J. Infrared and Raman spectroscopy of cellulose. *In Cellulose Chemistry and Technology, American Chemical Society* **1977**, *48*, 206−218.
(29) Cael, J.; Gardner, K.; Koenig, J.; Blackwell, J. Infrared and Raman spectroscopy of carbohydrates. Paper V. Normal coordinate analysis of cellulose I. *J. Chem. Phys.* **1975**, *62* (3), 1145−1153.
(30) Makarem, M.; Lee, C. M.; Kafle, K.; Huang, S.; Chae, I.; Yang, H.; Kubicki, J. D.; Kim, S. H. Probing cellulose structures with vibrational spectroscopy. *Cellulose* **2019**, *26* (1), 35−79.
(31) Xu, F.; Yu, J.; Tesso, T.; Dowell, F.; Wang, D. Qualitative and quantitative analysis of lignocellulosic biomass using infrared techniques: A mini-review. *Appl. Energy* **2013**, *104*, 801−809.
(32) Barnette, A. L.; Bradley, L. C.; Veres, B. D.; Schreiner, E. P.; Park, Y. B.; Park, J.; Park, S.; Kim, S. H. Selective detection of crystalline cellulose in plant cell walls with sum-frequency-generation (SFG) vibration spectroscopy. *Biomacromolecules* **2011**, *12* (7), 2434−9.
(33) Huang, S.; Makarem, M.; Kiemle, S. N.; Hamedi, H.; Sau, M.; Cosgrove, D. J.; Kim, S. H. Inhomogeneity of Cellulose Microfibril Assembly in Plant Cell Walls Revealed with Sum Frequency Generation Microscopy. *J. Phys. Chem. B* **2018**, *122* (19), 5006−5019.
(34) Huang, S.; Makarem, M.; Kiemle, S. N.; Zheng, Y.; He, X.; Ye, D.; Gomez, E. W.; Gomez, E. D.; Cosgrove, D. J.; Kim, S. H. Dehydration-induced physical strains of cellulose microfibrils in plant cell walls. *Carbohydr. Polym.* **2018**, *197*, 337−348.
(35) Lambert, A. G.; Davies, P. B.; Neivandt, D. J. Implementing the Theory of Sum Frequency Generation Vibrational Spectroscopy: A Tutorial Review. *Appl. Spectrosc. Rev.* **2005**, *40* (2), 103−145.

https://dx.doi.org/10.1021/acs.jpcb.0c07076
J. Phys. Chem. B 2020, 124, 8071−8081

(36) Wang, H. F.; Gan, W.; Lu, R.; Rao, Y.; Wu, B. H. Quantitative spectral and orientational analysis in surface sum frequency generation vibrational spectroscopy (SFG-VS). *Int. Rev. Phys. Chem.* **2005**, *24* (2), 191−256.
(37) Boyd, R. W.; Boyd, R. W. *Nonlinear Optics*; Elsevier Science: Burlington, VA, 2003.
(38) Shen, Y.-R. *The principles of nonlinear optics*; Wiley-Interscience: New York, 1984; Vol. 575, p 1984.
(39) Lee, C. M.; Chen, X.; Weiss, P. A.; Jensen, L.; Kim, S. H. Quantum Mechanical Calculations of Vibrational Sum-Frequency-Generation (SFG) Spectra of Cellulose: Dependence of the CH and OH Peak Intensity on the Polarity of Cellulose Chains within the SFG Coherence Domain. *J. Phys. Chem. Lett.* **2017**, *8* (1), 55−60.
(40) Lee, C. M.; Kubicki, J. D.; Fan, B.; Zhong, L.; Jarvis, M. C.; Kim, S. H. Hydrogen-bonding network and OH stretch vibration of cellulose: Comparison of computational modeling with polarized IR and SFG spectra. *J. Phys. Chem. B* **2015**, *119* (49), 15138−49.
(41) Lee, C. M.; Kafle, K.; Park, Y. B.; Kim, S. H. Probing crystal structure and mesoscale assembly of cellulose microfibrils in plant cell walls, tunicate tests, and bacterial films using vibrational sum frequency generation (SFG) spectroscopy. *Phys. Chem. Chem. Phys.* **2014**, *16* (22), 10844−53.
(42) Gray, D. G. Isolation and handedness of helical coiled cellulosic thickenings from plant petiole tracheary elements. *Cellulose* **2014**, *21* (5), 3181−3191.
(43) Lee, C. M.; Kafle, K.; Huang, S.; Kim, S. H. Multimodal broadband vibrational sum frequency generation (MM-BB-V-SFG) spectrometer and microscope. *J. Phys. Chem. B* **2016**, *120* (1), 102−16.
(44) Baudrier-Raybaut, M.; Haïdar, R.; Kupecek, P.; Lemasson, P.; Rosencher, E. Random quasi-phase-matching in bulk polycrystalline isotropic nonlinear materials. *Nature* **2004**, *432*, 374.
(45) Terrett, O. M.; Lyczakowski, J. J.; Yu, L.; Iuga, D.; Franks, W. T.; Brown, S. P.; Dupree, R.; Dupree, P. Molecular architecture of softwood revealed by solid-state NMR. *Nat. Commun.* **2019**, *10* (1), 4978.
(46) Rivard, M.; Popov, K.; Couture, C.-A.; Laliberté, M.; Bertrand-Grenier, A.; Martin, F.; Pépin, H.; Pfeffer, C. P.; Brown, C.; Ramunno, L.; Légaré, F. Imaging the noncentrosymmetric structural organization of tendon with Interferometric Second Harmonic Generation microscopy. *J. Biophotonics* **2014**, *7* (8), 638−646.
(47) Rivard, M.; Couture, C.-A.; Miri, A. K.; Laliberté, M.; Bertrand-Grenier, A.; Mongeau, L.; Légaré, F. Imaging the bipolarity of myosin filaments with Interferometric Second Harmonic Generation microscopy. *Biomed. Opt. Express* **2013**, *4* (10), 2078−2086.
(48) Han, Y.; Raghunathan, V.; Feng, R.-r.; Maekawa, H.; Chung, C.-Y.; Feng, Y.; Potma, E. O.; Ge, N.-H. Mapping Molecular Orientation with Phase Sensitive Vibrationally Resonant Sum-Frequency Generation Microscopy. *J. Phys. Chem. B* **2013**, *117* (20), 6149−6156.
(49) Sun, S.; Bisson, P. J.; Bonn, M.; Shultz, M. J.; Backus, E. H. G. Phase-Sensitive Sum-Frequency Generation Measurements Using a Femtosecond Nonlinear Interferometer. *J. Phys. Chem. C* **2019**, *123* (12), 7266−7270.
(50) Ma, D.; Lee, C. M.; Chen, Y.; Mehta, N.; Kim, S. H.; Liu, Z. Vibrational sum frequency generation digital holography. *Appl. Phys. Lett.* **2017**, *110* (25), 251601.
(51) Makarem, M.; Sawada, D.; O'Neill, H. M.; Lee, C. M.; Kafle, K.; Park, Y. B.; Mittal, A.; Kim, S. H. Dependence of sum frequency generation (SFG) spectral features on the mesoscale arrangement of SFG-active crystalline domains interspersed in SFG-inactive matrix: A case study with cellulose in uniaxially aligned control samples and alkali-treated secondary cell walls of plants. *J. Phys. Chem. C* **2017**, *121* (18), 10249−10257.
(52) Zhang, T.; Mahgsoudy-Louyeh, S.; Tittmann, B.; Cosgrove, D. J. Visualization of the nanoscale pattern of recently-deposited cellulose microfibrils and matrix materials in never-dried primary walls of the onion epidermis. *Cellulose* **2014**, *21* (2), 853−862.
(53) Zhang, T.; Vavylonis, D.; Durachko, D. M.; Cosgrove, D. J. Nanoscale movements of cellulose microfibrils in primary cell walls. *Nat. Plants* **2017**, *3* (5), 17056.
(54) Kafle, K.; Xi, X.; Lee, C. M.; Tittmann, B. R.; Cosgrove, D. J.; Park, Y. B.; Kim, S. H. Cellulose microfibril orientation in onion (Allium cepa L.) epidermis studied by atomic force microscopy (AFM) and vibrational sum frequency generation (SFG) spectroscopy. *Cellulose* **2014**, *21* (2), 1075−1086.
(55) Barnette, A. L.; Lee, C.; Bradley, L. C.; Schreiner, E. P.; Park, Y. B.; Shin, H.; Cosgrove, D. J.; Park, S.; Kim, S. H. Quantification of crystalline cellulose in lignocellulosic biomass using sum frequency generation (SFG) vibration spectroscopy and comparison with other analytical methods. *Carbohydr. Polym.* **2012**, *89* (3), 802−9.
(56) Lee, C. M.; Kafle, K.; Belias, D. W.; Park, Y. B.; Glick, R. E.; Haigler, C. H.; Kim, S. H. Comprehensive analysis of cellulose content, crystallinity, and lateral packing in Gossypium hirsutum and Gossypium barbadense cotton fibers using sum frequency generation, infrared and Raman spectroscopy, and X-ray diffraction. *Cellulose* **2015**, *22* (2), 971−989.
(57) Nishiyama, Y. P. J.; Jean, B.; Heux, L. *Ordering of cellulose microcrystals dispersed in polar and nonpolar medium*; ESRF, 2006.
(58) Barhoumi Meddeb, A.; Chae, I.; Han, A.; Kim, S. H.; Ounaies, Z. Magnetic field effects on cellulose nanocrystal ordering in a non-aqueous solvent. *Cellulose* **2020**. DOI: 10.1007/s10570-020-03320-5
(59) Ogawa, Y.; Lee, C. M.; Nishiyama, Y.; Kim, S. H. Absence of Sum Frequency Generation in Support of Orthorhombic Symmetry of α-Chitin. *Macromolecules* **2016**, *49* (18), 7025−7031.
(60) Kong, L.; Lee, C.; Kim, S. H.; Ziegler, G. R. Characterization of starch polymorphic structures using vibrational sum frequency generation spectroscopy. *J. Phys. Chem. B* **2014**, *118* (7), 1775−83.
(61) Rocha-Mendoza, I.; Yankelevich, D. R.; Wang, M.; Reiser, K. M.; Frank, C. W.; Knoesen, A. Sum Frequency Vibrational Spectroscopy: The Molecular Origins of the Optical Second-Order Nonlinearity of Collagen. *Biophys. J.* **2007**, *93* (12), 4433−4444.

https://dx.doi.org/10.1021/acs.jpcb.0c07076
J. Phys. Chem. B 2020, 124, 8071−8081